Image Transmission under Arctic Mirage Conditions

By Waldemar H. Lehn and H. Leonard Sawatzky *

Summary: The arctic mirage, an optical effect fairly common in the high latitudes, occurs when the atmosphere exhibits greater-than-normal refractive capability. Light rays then follow paths concave toward the earth, with curvature greater than or equal to that of the earth. The atmosphere acquires this refractive capability under conditions of temperature inversion, which exaggerate the fall-off of density (and hence refractive index) with elevation.

Equations are presented that calculate density profile from any given temperature profile; these results are used to develop ray path equations for nearly horizontal rays in the lower atmosphere. Ray paths are computed for two distinct mirage conditions (a strong shallow inversion and a mild but deep inversion) as well as for the standard atmosphere. With the aid of these paths, the appearance of the environment is shown. The strong inversion produces the appearance of a saucer-shaped earth (with image distortion near the horizon), whereas the mild inversion produces a "flat earth" appearance that permits great viewing distances.

Zusammenfassung: Die arktische Fata Morgana ist ein verhältnismäßig häufig vorkommender optischer Effekt in höheren Breiten. Er entsteht, wenn durch gesteigerte Densitätsschichtung der Atmosphäre Lichtstrahlbahnen gebrochen werden in einem Ausmaß, das der Krümmung der Erde gleicht oder sie überschreitet. Die Atmosphäre gewinnt diese Refraktionsfähigkeit unter Temperaturinversionsverhältnissen, welche die normale Densitätsabnahme mit zunehmender Höhe verstärken.

Gleichungen, die das Densitätsprofil bei gegebenem Temperaturprofil errechnen lassen, werden vorgelegt. Aus den Ergebnissen lassen sich Bahn-Gleichungen annähernd horizontaler Lichtstrahlen im bodennahen Raum entwickeln. Lichtstrahlbahnen werden als Beispiele berechnet und dargestellt, sowohl für eine flache, jedoch starke, und eine weniger starke, aber tiefe Inversion, als auch bezüglich der normalen Atmosphäre. Mit Hilfe dieser Ergebnisse wird die optische Gestalt der Umwelt errechnet. Die starke Inversion ergibt den Aspekt einer schüsselförmigen Erde; die weniger starken den einer absolut flachen Erde. Beide Erscheinungen verursachen eine optische Ausdehnung des Blickfeldes bei weit zurückweichendem Horizont.

1. *Introduction*

The arctic mirage is an optical phenomenon that occurs fairly frequently in the high latitudes. The effect, also called "loom" or "superrefraction", occurs when the atmosphere refracts light rays more strongly than usual. Under these conditions ray paths become concave toward the earth, with radii of curvature less than or equal to the earth's radius. Visual information can then be transmitted beyond the normal "horizon distance", and the surface takes on a flat or saucer-shaped appearance. This paper describes the physical basis for the mirage, and develops equations useful in predicting the appearance of the environment under mirage conditions.

Even the normal atmosphere refracts rays mildly, due to the decreasing density (and hence refractive index) with altitude. The effect is accentuated to produce the arctic mirage when a warm air mass rests upon a cold surface. The conductive cooling from below develops a temperature inversion, with a steeper-than-normal density gradient. This gradient in turn produces the stronger refraction effects that create the arctic mirage. This refracting layer need not be in contact with the earth's surface. The situation where warm air overlies cold air is equally effective, the necessary density gradient occuring in the boundary zone between the two layers. Hobbs reports that, in the high latitudes, the cold layer is frequently of the order of 1000 meters deep.

It should be noted that the arctic mirage is fundamentally distinct from the fata morgana or desert mirage, which depends on the opposite physical effect, namely pronounced heating of the air in contact with the earth's surface.

The following sections develop the equations that permit calculation of ray paths when the temperature profile in the lower atmosphere is known.

* Prof. Waldemar H. Lehn, Faculty of Engineering, University of Manitoba, Winnipeg, Man. R3T 2N2 (Canada). Dr. H. Leonard Sawatzky, Department of Georgraphy, University of Manitoba, Winnipeg, Man. R3T 2N2 (Canada).

2. *Ray paths in the refracting atmosphere*

The refractive effects of the atmosphere are well known. For visible light Bertram gives the refractive index as a function of density ρ (kg/m^3) by

$$n = 1 + (226 \times 10^{-6})\,\rho \tag{1}$$

and the propagation velocity v by

$$v = c/n \tag{2}$$

where c is the velocity of light in vacuum. In the following analysis the atmosphere is considered to be laterally homogeneous, so that the only spatial variation in density comes with elevation z above the earth's surface. Attention will be concentrated on rays whose paths remain close to the surface; an analogous development can be used to analyse refractive zones at higher elevations.

For such an atmosphere over a flat earth, Bertram derives an expression for the radius of curvature r at an arbitrary point on the ray:

$$\frac{1}{r} = \frac{\sin\theta(z)}{v(z)}\,\frac{dv}{dz} \tag{3}$$

where $\theta(z)$ is the angle between the ray and the vertical and v(z) is the velocity of propagation, at elevation z. From Snell's Law of Refraction, the term $(\sin\theta)/v$ is a constant for any given ray. Coordinates are chosen such that the ray is contained in the xz plane. An additional set of coordinates (see Fig. 1) facilitates further calculations: a new abscissa u is chosen tangent to the ray path at its starting point, and a new ordinate w pointing downward in the plane of the ray. On the basis that ray curvature is very small in the atmosphere, some approximations may be made:

$$x \simeq u \sin\theta$$

$$z \simeq z_o + u\cos\theta$$

$$\left|\frac{dw}{du}\right| << 1.$$

Hence in the uw coordinates the curvature expression becomes

$$\frac{1}{r} = \frac{\frac{d^2w}{du^2}}{\left[1 + \left(\frac{dw}{du}\right)^2\right]^{1.5}} \simeq \frac{d^2w}{du^2} \tag{4}$$

which combines with (3) to give

$$\frac{1}{r} = \frac{d^2w}{du^2} = \frac{\sin\theta}{v}\,\frac{dv}{dz}\,. \tag{5}$$

In the following paragraphs the path equation for nearly horizontal rays will be derived, as a function of propagation-velocity gradient dv/dz.

As the altitude variation of such rays is small, a Taylor expansion of dv/dz is useful:

$$\frac{dv}{dz} = v_o' + v_o''(z - z_o) + \frac{1}{2}v_o'''(z - z_o)^2 + \ldots \tag{6}$$

where the prime denotes differentiation with respect to z. Substitution of (6) into (5) yields

$$\frac{d^2w}{du^2} \simeq \frac{\sin\theta_o}{v_o}\left(v_o' + v_o''(z - z_o) + \frac{1}{2}v_o'''(z - z_o)^2\right). \tag{7}$$

Here the starting-point values θ_o, v_o are used for the constant ratio $(\sin\theta)/v$.

Following Bertram, one can now include the effects of the earth's curvature. For horizontal distances under 1000 km, the equation of the earth's surface is very closely

$z = -x^2/2R$, where R is the radius of the earth. In (7), the ray elevation above the surface will thus increase by the additional term $x^2/2R$. Secondly, the angle θ_o between ray and local vertical will decrease by the amount x/R. Incorporation of these effects into (7) produces an equation valid over the spherical earth:

$$\frac{d^2w}{du^2} = \frac{\sin(\theta_o - x/R)}{v_o}\left(v_o' + v_o''(z + \frac{x^2}{2R} - z_o) + \frac{v_o'''}{2}(z + \frac{x^2}{2R} - z_o)^2\right). \tag{8}$$

This equation must now be re-written in terms of uw coordinates. For nearly horizontal rays,

$$\left.\begin{aligned} x &\simeq u \\ \text{and } z &\simeq z_o + u\cos\theta_o - \frac{u^2}{2r_o}. \end{aligned}\right\} \tag{9}$$

The last term in the z-equation represents the effect of ray curvature: r_o is the radius of curvature at $u = 0$. The r_o term can be replaced using (5):

$$z \simeq z_o + u\cos\theta_o - \frac{v_o'\sin\theta_o}{2v_o}u^2. \tag{10}$$

Further, the sine function in (8) is expanded in a Taylor series, with ϕ_o defined as the complement of θ_o:

$$\sin(\theta_o - \frac{x}{R}) \simeq \sin\theta_o - \frac{u}{R}\sin\phi_o. \tag{11}$$

Equations (9), (10), (11) are substituted into (8) to give the differential equation for the ray path:

$$\begin{aligned} \frac{d^2w}{du^2} = \frac{(\sin\theta_o - \frac{u}{R}\sin\phi_o)}{v_o}\Bigg[v_o' + v_o''\left(u\sin\phi_o - \frac{v_o'\sin\theta_o}{2v_o}u^2 + \frac{u^2}{2R}\right) \\ + \frac{v_o'''}{2}\left(u\sin\phi_o - \frac{v_o'\sin\theta_o}{2v_o}u^2 + \frac{u^2}{2R}\right)^2\Bigg]. \end{aligned} \tag{12}$$

This equation is integrated twice to produce the equation of the ray path in the uw coordinate system. In each coefficient of u^n, any terms at least 1000 times smaller than their neighbours have been neglected.

$$\begin{aligned} w = \frac{\sin\theta_o}{v_o}\Bigg[\frac{v_o'}{2}u^2 + \frac{v_o''\sin\phi_o}{6}u^3 + \frac{1}{12}\left(\frac{v_o''}{2R} - \frac{v_o'v_o''\sin\theta_o}{2v_o} + \frac{v_o'''\sin^2\phi_o}{2}\right)u^4 \\ + \frac{1}{20}\left(\frac{v_o'''\sin\phi_o}{2R} - \frac{v_o'v_o'''\sin\phi_o\sin\theta_o}{2v_o}\right)u^5 + \frac{v_o'''}{60}\left(\frac{v_o'^2\sin^2\theta_o}{4v_o^2} + \frac{1}{4R^2} - \frac{v_o'\sin\theta_o}{2v_oR}\right)u^6\Bigg] \end{aligned} \tag{13}$$

The subscripts "o" refer to values at the origin of the uw coordinates.
Typical orders of magnitude for the velocity derivatives are $v'_o \simeq 100\ \text{sec}^{-1}$, $v_o'' \simeq 10\ \text{m}^{-1}\text{sec}^{-1}$, and $v_o''' \simeq 1\ \text{m}^{-2}\text{sec}^{-1}$.

3. *Relation between velocity gradient and temperature profile*

The path equation (13) requires the derivatives of propagation velocity with respect to elevation. These derivatives may be calculated from a given temperature profile as follows. A standard result in elementary physics is the equation for pressure in an atmosphere situated in a gravitational field:

$$\frac{dp}{dz} = -g\rho(z) \tag{14}$$

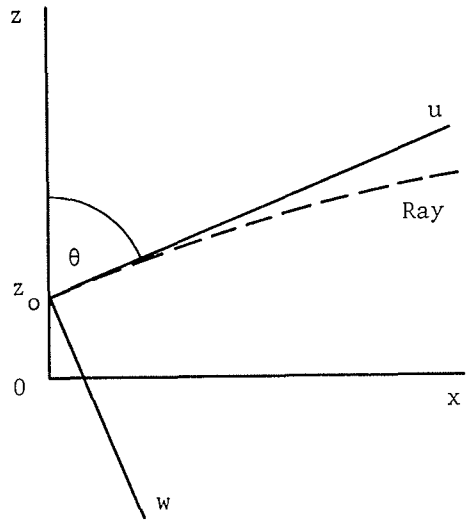

Fig. 1: Choice of coordinate systems.
Abb. 1: Wahl der Koordinatensysteme.

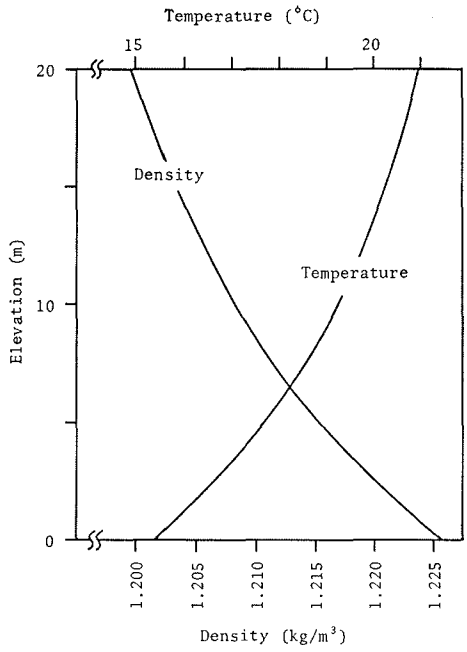

Fig. 2: Temperature and density profiles: example of strong inversion.
Abb. 2: Temperatur- und Dichteprofile: Beispiel einer starken Inversion.

where p is the pressure at elevation z, and g is the acceleration of gravity (assumed constant over the range of elevations to be encountered). Further, representing the behaviour of air for small deviations from standard temperature and pressure by the ideal gas equation pV = nRT, one can write the density as

$$\rho = \frac{\beta p}{T} \tag{15}$$

where T is the temperature in degrees K and β is a constant of proportionality. For the Standard Atmosphere of the Air Research and Development Command (see Mizner et al.) the value of β is about $3.49 \cdot 10^{-3}$ MKS units. Table 1 summarises some pertinent values for this atmosphere.

Atmospheric pressure at earth's surface:	$p_o = 1.013 \cdot 10^5$ n/m²
Surface density of air at 15° C:	$\rho_o = 1.225$ kg/m³
Effective molecular weight of air:	29.0
Radius of the earth:	R = 6400 km
Velocity of light in vacuum:	$c = 3 \cdot 10^8$ m/sec.

Tab. 1: Numerical values used in calculations.
Tab. 1: Bei der Berechnung benutzte Werte.

Substitution of (15) into (14) produces an equation that can be integrated; the result is

$$\int_{p_o}^{p(z)} \frac{dp'}{p'} = -g\beta \int_o^z \frac{dz'}{T(z')} . \tag{16}$$

The solution for p(z) is thus

$$p(z) = p_o \exp\left[-g\beta \int_o^z \frac{dz'}{T(z')}\right] \tag{17}$$

which when substituted back into (15) permits the calculation of density ρ (z) when the temperature profile T(z) is known:

$$\rho(z) = \frac{\beta p_o}{T(z)} \exp\left[-g\beta \int_o^z \frac{dz'}{T(z')}\right]. \tag{18}$$

The remaining step, from density to propagation velocity, is straightforward. Equations (1) and (2) combine to give

$$v = \frac{c}{1 + 0.000226\,\rho} \tag{19}$$

which to an accuracy better than one part in a thousand is equivalent to

$$v = c\,(1 - 0.000226\,\rho)\,. \tag{20}$$

Differentiation of (20) yields the velocity derivatives in terms of the density derivatives. The path equations were solved by a numerical procedure, the details of which are outlined below *.

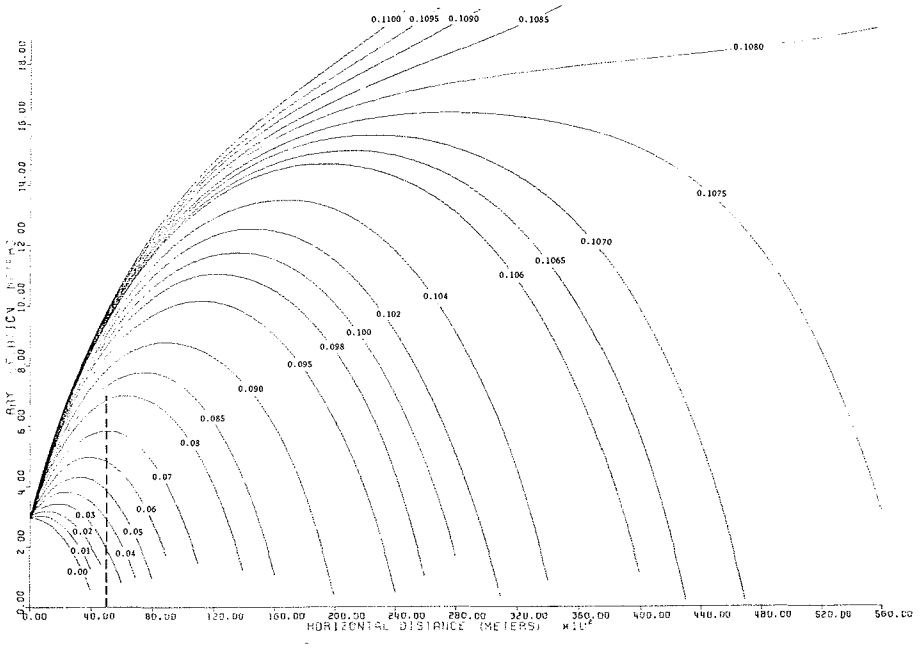

Fig. 3: Ray paths for conditions of strong temperature inversion. Ray elevation above the earth's surface is plotted against distance along the surface. The observer's eye is 3 meters above the surface. The numbers on the paths give ray angles, in degrees above the horizontal, at the observer's station.

Abb. 3: Lichtstrahlbahnen bei starker Temperaturinversion: die Höhe der Strahlbahn über der Erdoberfläche ist gegenüber der linearen Entfernung vom Ausgangspunkt dargestellt. Das Auge des Beobachters ist in 3 m Höhe. Die Aufschriften geben den Winkel eines Strahles zur Horizontalebene (in °) an, vom Standpunkt des Beobachters betrachtet.

*) The computational procedure used to calculate the ray paths will be briefly outlined. First a density table (equation [18]) at 4-meter intervals is calculated from the temperature profile data. To find the velocity derivatives at any elevation, a cubic polynomial is fitted to the neighbouring density points. Differentiation of this cubic (and use of equation [20]) gives the velocity derivatives. Ray path computations then proceed in uw coordinates according to (13) until the u^6 term exceeds 0.001 m, at which time a new uw system is chosen. This shift of origin must be done carefully; as the new z-axis is not exactly parallel to the original one (earth's curvature) a corresponding correction must be applied to the new value of ϕ_0. Ray elevation above the earth's surface (assumed free of irregularities) is found by returning to xz coordinates and using the relation $z = -x^2/2R$ to represent the earth's surface. The whole procedure is repeated until the ray intersects the earth or goes beyond the area of interest.

Elevation m	Temperature °C	Elevation m	Density kg/m³
0.0	15.37	0.0	1.226
0.8	15.8	4.0	1.217
2	16.4	8.0	1.211
8.0	18.7	12.0	1.206
16.0	20.4	16.0	1.203
24.0	21.34	20.0	1.200
		24.0	1.198

Tab. 2: Temperature and density data for example of strong inversion.
Tab. 2: Temperatur- und Dichtewerte für das Beispiel einer starken Inversion.

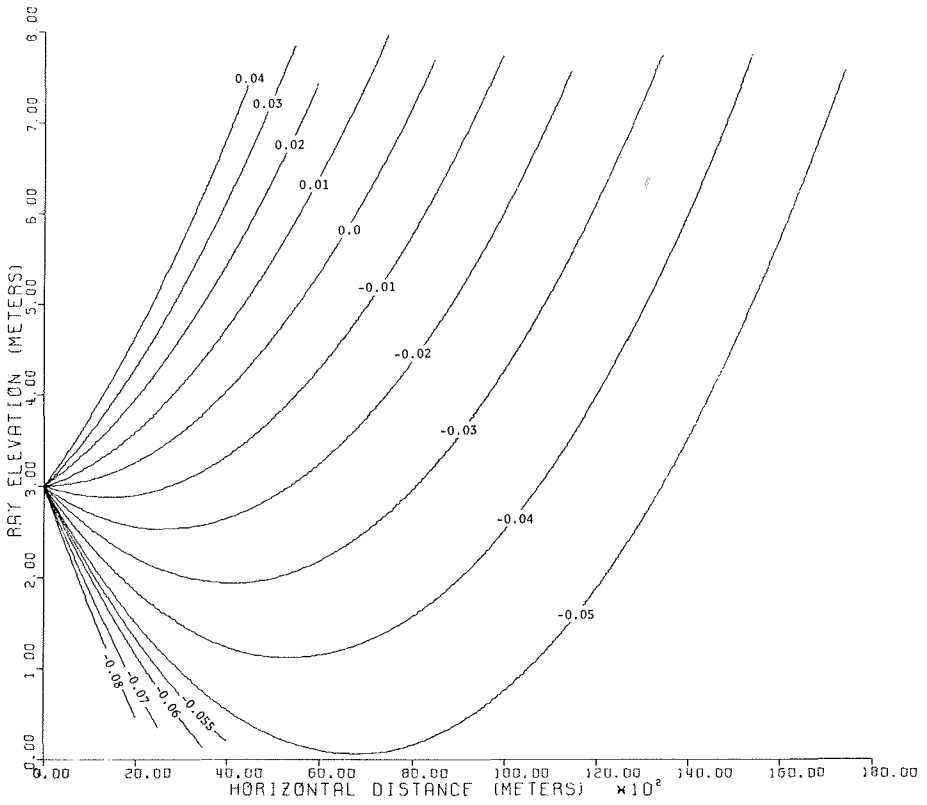

Fig. 4: Ray paths for the standard atmosphere. The numbers indicate angles (in degrees above horizontal) at the observer's eye, which is 3 meters above the surface.
Abb. 4: Bahnen der Lichtstrahlen in der genormten Atmosphäre: die Aufschriften geben den Winkel zur Horizontalebene (in °) vom Standpunkt des Beobachters (3 m Höhe) an.

4. *Appearance of environment under strong temperature inversion*

Strong inversions can appear when the atmosphere is conductively cooled from below, as occurs in overnight radiation cooling of the ground, or when warm air lies over cold water. An example of strong inversion was chosen from measurement data collected in Lettau and Davidson; Fig. 2 and Table 2 present the associated temperature and density profiles. Lyons records inversions of similar intensity. With the observer's eye at an elevation of 3 meters, the ray paths shown in Fig. 3 were computed. This figure permits one to reconstruct the appearance of the environment under these conditions. For comparison purposes Fig. 4 shows the ray paths for the standard atmosphere. The strength

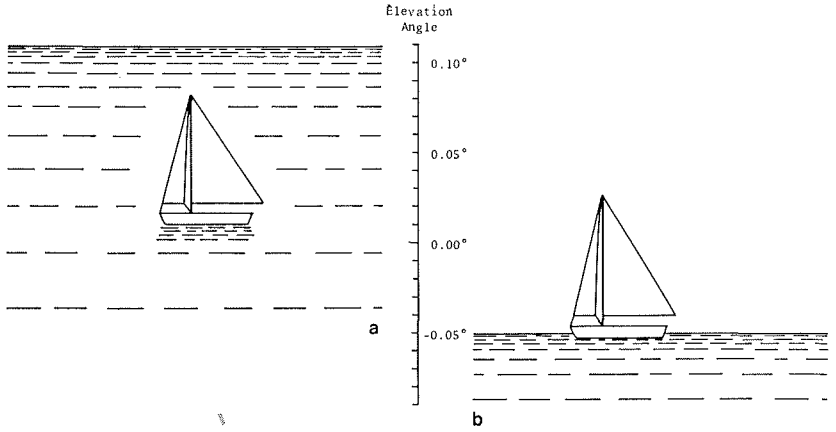

Fig. 5: Aspect of a sailboat under conditions of strong inversion (a) and standard atmosphere (b). The tip of the mast is 7 meters above the waterline, while the deck is 0.6 meter above the water; length of the boat is 4.5 meters. The vertical scale gives angles subtended at the observer's eye, which is 3 meters above the water surface.

Abb. 5: Aspekte eines Segelbootes unter Verhältnissen einer starken Inversion (a) bzw. genormter Atmosphäre (b): die Spitze des Mastes ragt 7 m über die Wasserfläche, das Deck 0,6 m. Die Länge des Boots ist 4,5 m. Die senkrechte Skala gibt die Winkel zwischen der Horizontalebene und dem Ausgangspunkt des Lichtstrahls, vom Standpunkt des Beobachters in 3 m Höhe über der Wasserfläche aus gesehen.

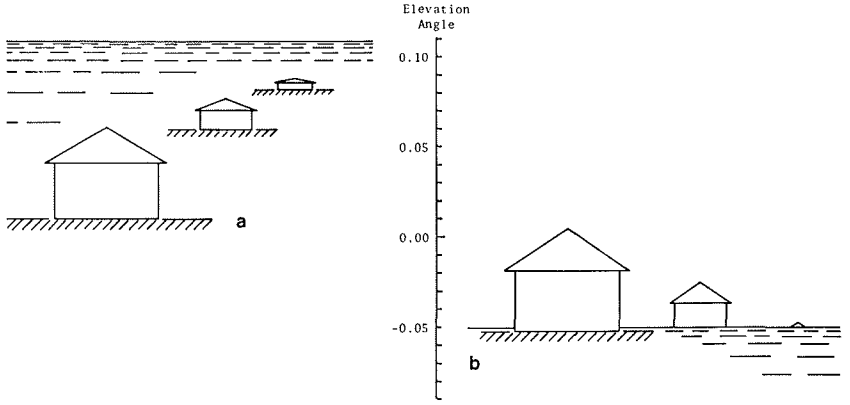

Fig. 6: Aspect of buildings on very flat ground under conditions of strong inversion (a) and standard atmosphere (b). The buildings, all of the same dimensions, are respectively 5, 10, and 15 km from the observer, whose eye is 3 meters above the ground. The buildings are 5 meters wide; the rooftop and eaves are respectively 5 and 3 meters above the ground.

Abb. 6: Aspekte von Gebäuden auf flachem Gelände unter Verhältnissen starker Inversion (a) bzw. genormter Atmosphäre (b): Die Gebäude, von genau gleichmäßiger Größe, stehen in 5, 10 und 15 km Entfernung vom Beobachter, dessen Auge sich in 3 m Höhe befindet. Die Gebäude sind 5 m breit; die Giebel und Dachkanten ragen 5 m bzw. 3 m über die Erdoberfläche.

of the effect seen by the observer is emphasized by the presence of familiar references in the field of view. To illustrate this, an over-water view of a small sailboat 5 km from the observer was chosen. The dotted vertical line on Fig. 3 shows the location and size of the boat. The aspect of the boat is drawn to scale in Fig. 5, where Fig. 5a is for the conditions of strong inversion, and Fig. 5b for the standard atmosphere. The reference scale represents the angle subtended at the unaided eye. Note that in Fig. 5a the horizon

is clearly higher than the top of the mast, leaving the viewer with the distinct impression that the earth's surface is saucer-shaped.

Fig. 6 shows a similar situation over extremely flat ground, as exemplified by the Lake Agassiz plain in southern Manitoba (the inhabitants of this area are familiar with these visual effects). The situation illustrated represents three villages at distances of 5, 10 and 15 km respectively from the observer. Under the mirage conditions (Fig. 6a) the villages appear "staircased" one above the other, and the horizon is higher than all of them. An image distortion that increases with distance also becomes apparent, due to compression of ray paths as the horizon is approached: rays originating at progressively farther points subtend progressively smaller angles at the observer's eye. In the normal view, on the other hand, the first village stands much higher than the second, and the third barely rises over the horizon.

5. Conditions for viewing great distances

For a line of sight of maximum length, the ray path must have a radius of curvature equal to that of the earth. For a surface temperature of 0° C, the requisite temperature gradient was found to be 0.112° C per meter. Fig. 7 shows the resulting ray paths, assuming the somewhat idealised case for which the inversion layer with this gradient has a 50-meter depth. As a specific example, an object 50 m high located 200 km from the observer subtends an angle of about 1/3 minute of arc. Under conditions of good illumination and contrast, such an object is visible to the naked eye.

In a stable inversion layer of unlimited extent, the ultimate limit on viewing distance would be set by light absorption in the atmosphere. The appendix gives the formula for the appropriate transmission factor. Image transmission near the earth's surface is feasible up to 400 km, of sufficient quality that the unaided eye could derive useful information from it. If the image is transmitted at higher levels in the atmosphere, as occurs when the refracting layer is at the upper boundary of a deep cold-air layer, the image quality is improved: the thinner air at the upper levels absorbs less light, so that more of the light leaving the object reaches the observer. Stefansson reports a well-authenticated, clear viewing of Snaefells Jökull in Western Iceland from a position at

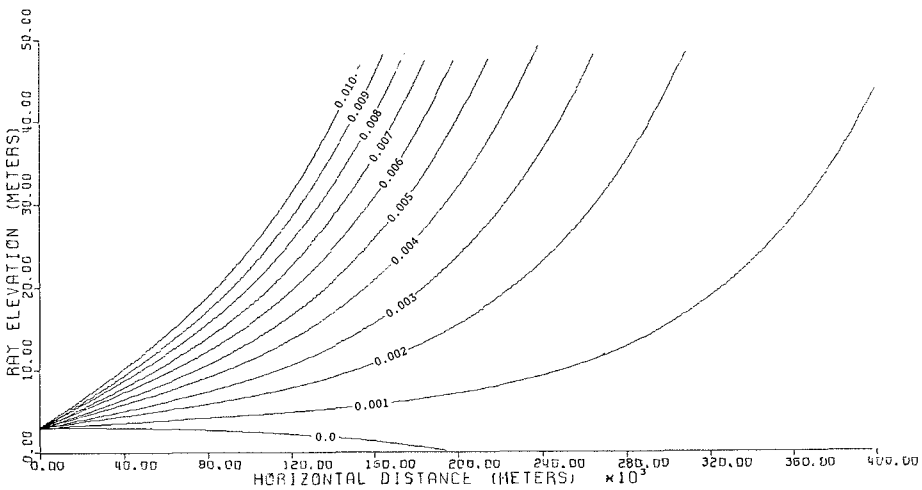

Fig. 7: Ray paths that permit very large viewing distances. The numbers indicate angles (in degrees above horizontal) at the observer's eye, 3 meters above the surface.

Abb. 7: Bahnen der Lichtstrahlen, die gesteigerte Sichtweite ermöglichen. Die Aufschriften geben die Winkel (in °) zur Horizontalebene in 3 m Höhe an.

sea over 500 km distant; and Hobbs cites numerous cases in which lines of sight range from 300 to 400 km in length.

6. *Conclusions*

The arctic mirage occurs when a temperature inversion produces a steepened density gradient in the lower atmosphere. The preceding paragraphs give equations that relate temperature profile to density, and density profile to (nearly horizontal) ray paths. With the aid of these equations, the appearance of the environment can be predicted for any lower-atmosphere temperature profile.

The effects of the mirage are noticeable primarily over flat, relatively featureless terrain. For strong inversions near the surface the observer sees a saucer-shaped earth, with objects near the horizon somewhat distorted. On the other hand, viewing over very great distances is made possible by mild deep inversions, which when located near the surface produce the appearance of a flat earth.

Historical and cultural implications of the arctic mirage are examined in a separate paper. There the authors contend that the mirage may have had significant influence in the formation of the medieval world-image, and in early North Atlantic exploration. The mirage permitted the experienced but unsophisticated observer of the previous millenium to confirm theories of a flat or saucer-shaped world; in addition he could derive practical benefit from the mirage when it transmitted information from beyond the normal horizon.

References

Baur, F.: Meteorologisches Taschenbuch, Vol. II. Leipzig, Akademische Verlagsgesellschaft, 1970.

Bertram, S.: Compensating for Propagation Errors in Electromagnetic Measuring Systems. I.E.E.E. Spectrum, March 1971.

Hobbs, W. H.: Conditions of Exceptional Visibility within High Latitudes, Particularly as a Result of Superior Mirage. Annals of the American Association of Geographers, December 1937.

Lettau, H. H. and B. Davidson (ed.): Exploring the Atmosphere's First Mile; Proceedings of the Great Plains Turbulence Field Program. New York, Symposium Publications Division, Pergamon Press, 1957.

Lyons, W. A.: Numerical Simulation of Great Lakes Summertime Conduction Inversions. Proc. 13th Conference on Great Lakes Resources, 1970.

Mizner, R. A., K. S. W. Champion and H. L. Pond: The ARDC Model Atmosphere, 1959. Air Force Surveys in Geophysics, no. 115.

Moore, R. K.: Tropospheric Propagation Effects on Earth-Space Low Elevation Angle Paths. Lawrence, Kansas, U. of Kansas Publications, Bull. of Engineering No. 61, 1970.

Rossi, B.: Optics. Reading, Mass., Addison-Wesley Publishing Co., 1965.

Stefansson, V.: Ultima Thule. New York, N. Y., The Macmillan Co., 1940.

Appendix

The extinction coefficient, a, for dry air is given in Baur:

$$a = 1.061 \frac{8\pi^3}{3} \cdot \frac{(n_s^2 - 1)^2}{N_s^2 \lambda^4} \int_o^d N \, dx$$

where n_s = refractive index of air at S.T.P.,
N_s = number of air molecules per cubic centimeter at S.T.P.,
N = number of air molecules per cubic centimeter along ray path,
d = distance of object from observer,
λ = wavelength of radiation.

The light-transmission factor q is $q = \exp(-a)$. As a specific example, consider a path of length 200 km at a small, roughly constant elevation. For air temperature 0° C and light wavelength 0.6μ, the extinction coefficient is $a = 1.72$, and the transmission factor is $q \simeq 0.18$. Thus 18% of the light intensity originating at the object will reach the observer. A similar calculation for air at 15° C leads to the values $q \simeq 9\%$ for a 300 km path length, and $q \simeq 4\%$ for a 400 km path.